Soft Matter

Molecular Dynamics Studies of Entropic Elasticity of Condensed Lattice Networks Connected with Uniform Functionality *f* = 4

Journal:	*Soft Matter*
Manuscript ID	SM-ART-11-2021-001641
Article Type:	Paper
Date Submitted by the Author:	18-Nov-2021
Complete List of Authors:	Hagita, Katsumi; National Defense Academy, Department of Applied Physics Murashima, Takahiro; Tohoku University, Department of Physics

ARTICLE

Molecular Dynamics Studies of Entropic Elasticity of Condensed Lattice Networks Connected with Uniform Functionality $f = 4$

Received 00th January 20xx,
Accepted 00th January 20xx

DOI: 10.1039/x0xx00000x

Katsumi Hagita,*[a] and Takahiro Murashima[b]

To study the linear region of entropic elasticity, we considered the simplest physical model possible and extracted the linear entropic regime by using the least squares fit and the minimum of the mean absolute error. With regard to the effect of the fluctuation of the strand length N_s, the strand length with fluctuation was set to a form proportional to $(1.0 + C(R - 0.5))$, where R is a uniform random number between 0 and 1 and C is the amplitude of fluctuation. This form enabled us to analytically calculate the fluctuation dependence of the elastic modulus G. To reveal the linear regions of entropic elasticity as a function of the strand length between neighboring nodes in lattices, molecular dynamics (MD) simulations of condensed lattice networks with harmonic bonds without the excluded volume interactions were performed. Stress-strain curves were estimated by performing uniaxial stretching MD simulations under periodic boundary conditions with a bead number density of 0.85. First, we used a diamond lattice with functionality $f = 4$. The linear region of the entropic elasticity was found to become larger with the increasing number of beads in a strand N_s. For $N_s = 100$, the linear region had a strain of up to 8 for a regular diamond lattice. We investigated the effect of strand length fluctuation on the diamond lattice, and we confirmed that the equilibrium shear modulus G increases as the obtained analytical prediction and the linear entropic region in the stress-strain curves becomes narrower with increasing fluctuation of N_s. To investigate the difference in network topology with the same functionality f and uniform strand length N_s, we performed MD simulations on regular networks of the BC-8 structure with $f = 4$ prepared from the ab initio DFT calculations of carbon at high pressure. We found that the elastic behavior depends on the network connectivity (i.e., topology). This indicates that the network topology plays an important role in the emergence of nonlinearity owing to the crossover from entropic to energetic elasticity.

Introduction

Rubber elasticity has attracted increasing academic and industrial interest.[1-5] In particular, suitable molecular dynamics (MD) simulation methods and theories need to be developed for crosslinked rubbers that show linear entropic elasticity even under a large deformation. Theories could be evaluated and confirmed directly through large-scale MD simulations in which the spatial scale relations correspond to experimental ones.

Crosslinked polydimethylsiloxane (PDMS) rubbers can show linear elasticity over a wide strain region for strains exceeding 10.[6] For example, Sakai[7,8] and Shibayama[9,10] reported tetra-polyethylene glycol (PEG) gels with high stretchability. Nonetheless, the relationship between the network topology of crosslinked polymers and nonlinear behaviors must be clarified because some crosslinked rubbers exhibit nonlinear behaviors at lower strain regions. According to the foundational work of Pincus,[11] the excluded volume (EV) effect leads to the nonlinearity observed under high elongation when both ends are stretched further than the Flory radius of unperturbed coil. Recently, Katashima[12] confirmed that the extended Gent model in uniaxial and biaxial stretching measurements on Tetra-PEG gels. In biaxial stretching, the cross term due to the EV effect was significant. Contrarily, there was no cross-term contribution due to the EV effect in uniaxial elongation. Further, the EV effect was found to be essential in gel swelling.

For the uniaxial elongation of gels in solvents, the bond stretching effect owing to chain crossing prohibition was considered minor even in the high-strain region, although solvent-free rubber materials showed nonlinear elasticity in this region. Very recently, elastic polymer networks have been theoretically investigated while ignoring the EV effects[13-22]; however, direct confirmations through MD simulation have not been obtained. A simulation-based study can conclusively track the emerging nonlinear elasticity in the high-strain region as a function of chain length; therefore, we conducted large-scale MD simulations. As mentioned above, the threshold strains were expected to depend on the connectivity (topology) of the polymer network under the uniaxial elongation. Thus, theoretical studies have used models that allow chain crossing to investigate the elasticity of gels and/or rubbers. For example, Johnson et al.[13-15] extensively examined the topological effects on the polymer elasticity of real Gaussian phantom networks. They developed a real elastic network theory (RENT) to consider

[a] Department of Applied Physics, National Defense Academy, 1-10-20 Hashirimizu, Yokosuka 239-8686, Japan.
[b] Department of Physics, Tohoku University, 6-3, Aramaki-aza-Aoba, Aoba-ku, Sendai, 980-8578, Japan

† Footnotes relating to the title and/or authors should appear here.
Electronic Supplementary Information (ESI) available: [details of any supplementary information available should be included here]. See DOI: 10.1039/x0xx00000x

the effect of cyclic defects in the phantom network. Lang[16-20] studied the elasticity of polymer model networks with cyclic defects extensively. Panyukov[21,22] investigated the effects of loops in polymer networks.

These recent studies[13-22] have aimed to extend classical theories such as the affine network model (ANM)[23-25] and phantom network model (PNM)[26-28] to account for the effect of defects such as loops. Generally, the shear modulus G can be calculated as:

$$G = (\upsilon - h\mu)k_B T, \quad (1)$$

where ν and μ denote the number of elastically active strands and junctions in the network, respectively; k_B is the Boltzmann constant; T is the temperature; and h is a factor characterizing the model. For h = 0 and 1, Eq. (1) gives G for an ANM and a PNM, respectively. For PNM, by using the functionality f, Eq. (1) can be rewritten as $G_{PNM} = (1-2/f)\nu k_B T$.

In MD simulations, reproducing the linear entropic elasticity up to high strains is currently difficult. Among pioneering MD simulations of crosslinked networks, Everaers and Kremer[29-31] investigated the elastic modulus of a diamond lattice network, and Grest et al.[32,33] investigated that of an end-link gel with random crosslinking. To estimate the elastic properties of the Gaussian polymer networks of random end-link gels, Gusev et al.[34-36] performed MD simulations using two MD models: (1) harmonic bonds without the Lennard-Jones (LJ) interaction,[35] and (2) finite extensible nonlinear elastic (FENE) bonds with the LJ interaction restricted to nearest and next-nearest neighbor beads along the chains.[36] They estimated the shear modulus G from the terminal plateau behaviors of $G(t)$ and by fitting the nominal stress for a small strain region (*i.e.*, strain less than 1.1). Notably, they reviewed[35] the correspondence between typical rubbers and Kuhn monomers. Because a strand of typical rubbers had 100 − 1000 skeletal bonds and a Kuhn monomer had ~ 10 skeletal bonds, the strand of typical rubbers had ~ 10 − 100 Kuhn monomers. Based on this estimation, a network of up to 60 springs per strand was investigated.

Among theoretical studies that compared the shear moduli of regular lattices with f = 3, 4, 6, and 8, Toda and Morita[37] performed MD simulations of polymer chain models using FENE bonds with and without the excluded volume interactions. They obtained the equilibrium shear modulus G by fitting the nominal stress σ_n to the following approximated equation:

$$\sigma_n = G\left(\lambda - \frac{1}{\lambda^2}\right), \quad (2)$$

where λ is the strain (stretch ratio). The fitting region was expected to be limited because nonlinear behaviors arise from a function form of the FENE potential. In addition, the choice of the fitting region may be inconclusive because the dependence of stress values on the stretching rate in the low-strain region was not negligible, as reported in the present study. Because the strand length was not large enough in their work, the high stretching of the PDMS rubbers and tetra-PEG gels was not reproduced.

To reproduce the linear entropic elasticity of the PDMS rubbers and tetra-PEG gels under high strains, using a long strand length and avoiding artifacts due to a nonlinear spring were essential. Treloar[38] theoretically investigated the need for long chains to obtain a wide linear region for stretching. In the present study, MD simulations of polymer chain models were conducted using the linear spring of a harmonic potential without the EV effect. If MD simulations are performed without the EV effect for biaxial stretching and gel swelling, the results might be meaningless because the crossing prohibition is nonnegligible, as shown by Katashima et al.[12] By contrast, for theoretical studies of uniaxial elongation, MD calculations without the EV effect are meaningful to decompose and factorize several effects. In particular, understanding the emerging nonlinear elasticity in the high-strain region as a function of strand length provides insights to relate theoretical polymer networks to actual ones.

The remainder of this paper is organized as follows. The second section explains the simulation method for a polymer chain model of a linear spring. The third section presents analyses of the stress-strain relations of a regular diamond lattice with a unique strand length. The fourth section investigates regular diamond lattices with randomly fluctuating strand lengths. The fifth section discusses the typical behaviors of regular networks with different topologies. Finally, our conclusions are summarized in the last section.

Simulation method

In the present study, we performed coarse-grained (CG) MD simulations with a linear spring of a harmonic potential. For this purpose, we used the MD simulation software LAMMPS.[39]

In the present model, the pair potential for every pair of beads is given by:

$$U_{\text{pair}}(r) = 0, \quad (3)$$

where r is the distance between the beads. For bonded beads, the harmonic potential was applied:

$$U_{bond}(r) = K(r - r_0)^2, \quad (4)$$

where K = 40 ε/σ^2 is the spring constant, and r_0 is the natural bond length of the linear spring. For comparisons with other models, such as the Kremer-Grest model,[40] we set r_0 = 0.975 σ. The prepared polymer networks were placed in a box under periodic boundary conditions (PBCs) with a bead number density of 0.85. The bead dynamics in our model were described by the Langevin equation with a friction constant ζ = 0.5 m/τ and temperature T. Here, the unit of T is ε/k_B. The time scale is given by $\tau = \sigma(m/\varepsilon)^{1/2}$, where m is the mass of a monomer. The velocity Verlet algorithm was used for numerical integration of the Langevin equation with a time step Δt = 0.005 τ. For simplicity, we set $m = \varepsilon = \sigma = \tau$ = 1 hereafter.

For preparing polymer networks, we obtained the regular lattice of carbon from *ab initio* density functional theory (DFT) calculations using Quantum Espresso.[41] Diamond and BC-8 lattices[42-45] can be obtained under low and high pressures, respectively. The BC-8 structure had a backbone structure similar to a nested K4 lattice[46] (also recognized as a double

gyroid,[47,48] nested network of SRS,[49] etc.) which is known to be a double network with f = 3. To achieve a smaller energy at a high pressure, the carbon lattice was weakly deformed to produce sp3-bonds with f = 4. To make a polymer network, the sp3-bond of these carbon lattices was replaced by a strand with some number of beads (N_s). Because the lattice constant of the unit cell depends on the atomic species, DFT calculation is required to specify the lattice constant.

Figure 1 shows the lattice structure of the diamond and BC-8 lattices. Cross-sectional views of the BC-8 lattice reveal anisotropy in one direction. Here, the numbers of bonds and nodes (n_{bond} and n_{node}, respectively) in the unit cell of the diamond and BC-8 lattices were (n_{bond}, n_{node}) = (16, 8) and (32, 16), respectively. For n_{cell} unit cells, the total number of beads N_t is given by $n_{cell} \times (n_{bond} N_s + n_{node})$.

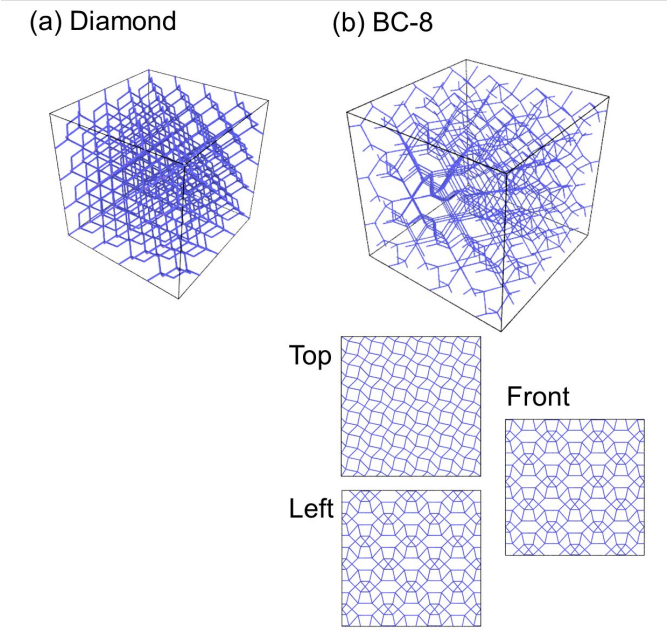

Fig. 1 Schematic view of (a) regular diamond and (b) BC-8 lattices.

Stress-strain relations of elongated diamond lattice network with uniform strand length

Stress-strain relations and estimation of linear region

First, we investigated the case with N_s = 100. For this system, N_t = 201,000. Figure 2 shows the stress-strain curves under a stretching rate of 10^{-5}. From a least square fit to Eq. (2), the fitted value of G was 0.0023821 for the strain range of 1.0 – 8.1, where the upper limit λ_u = 8.1 of the strain range was determined so as to minimize the mean absolute error (MAE). From Fig. 2, λ_u = 8.1 can be considered the onset of the nonlinear region.

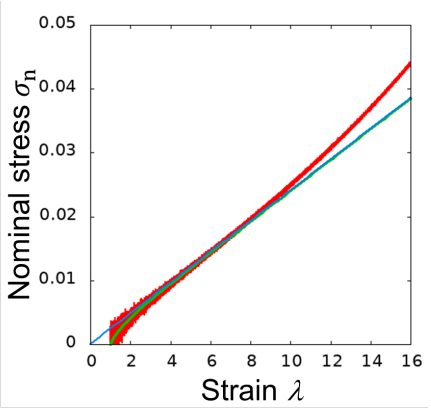

Fig. 2 Stress-strain curve of polymer network of regular diamond lattice with N_s = 100 under $d\lambda/dt = 10^{-5}$. Red line represents data points obtained from simulation; green line represents the fitting curve to Eq. (2); and blue line is a linear function.

The stretching rate of 10^{-4} was selected for this study because the difference between ($d\lambda/dt$ =) 10^{-4} and 10^{-5} is negligible, as illustrated in Appendix A. Additionally, for $d\lambda/dt$ = 10^{-3}, the apparent linear region appears to have widened due to poor fitting in the low-strain region. Furthermore, the $d\lambda/dt$ value of 10^{-4} corresponded to the G and λ_u values of 0.0024238 and 8.2, while the $d\lambda/dt$ value of 10^{-3} corresponded to the G and λ_u values of 0.0025207 and 11.5, respectively. These findings suggest that a sufficiently low stretching rate should be used to determine the upper limit λ_u.

We concentrated on a density ρ of 0.85 in this study because it is a common value for polymer melts described by the Kremer-Grest model.[40] Additionally, the stress-strain curves for the cases with ρ = 0.1 and 0.3 are presented in the Appendix C. Because decreasing the density expands the corresponding network, the apparent linear region becomes narrower as the value of ρ decreases. As a result, cases with ρ = 0.85 were primarily investigated.

Strand-length dependence of stress-strain relations

Based on a one-dimensional model of entropic elasticity, we considered that λ_u was roughly proportional to N_s for small N_s. From the CGMD of a stretched single chain with the phantom chain model with (K, r_0) = (40, 0.975), λ_u was obtained to be 5.0, 7.2, and 10.1 for N = 50, 100, and 200, respectively (see Appendix D). In addition to the properties of the spring, the network structure is expected to affect λ_u and non-linearity at high strain emerges owing to the crossover from entropic elasticity to energetic elasticity. To investigate the N_s dependence on the nonlinearity in the high-strain region, we investigated cases with N_s values of 50 and 200. For these systems, N_t was 174,528 and 205,312, respectively.

Figure 3 shows the stress-strain curve with $d\lambda/dt = 10^{-4}$ for N_s values of 50 and 200. The fitting to Eq. (2) provided (G, λ_u) = (0.0059993, 5.1) and (0.00097443, 14.2) for N_s = 50 and 200,

respectively. In principle, the low-strain region was expected to not depend on N_s, as given by Eq. (2). However, notably, the deviation due to stretching rate ($d\lambda/dt$) dependence increases as N_s increases owing to the relaxation time of the strand. It should be noted that λ_u may be roughly proportional to N_s. Further, the values of λ_u = 5.1, 8.2, and 14.2 for N = 50, 100, and 200 were clearly different from the values (5.0, 7.2, and 10.1) of a stretched single chain. We considered that the difference in the ratio of number of node points and chain particles has an effect, and detailed investigations and theoretical calculations of this behavior are in progress.

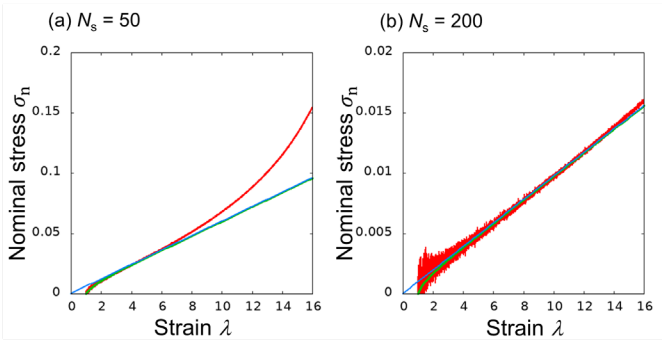

Fig. 3 Stress-strain curve of polymer network of regular diamond lattice with N_s = (a) 50 and (b) 200 under $d\lambda/dt = 10^{-4}$. Red line represents data points obtained from simulation; green line represents the fitting curve to Eq. (2); and blue line is a linear function.

Figure 4 shows the stress-strain curve for N_s = 50. This curve could be divided into four characteristic regions, as shown in Fig. 5: (1) a region depending on the stretching rate at low strain, (2) a region exhibiting linear entropic elasticity, (3) a crossover region between the entropic and energetic regions, and (4) a region characterizing the energetic elasticity. Estimations of the threshold values (lower and upper limits of linear region and lower limit of energetic elasticity region) are discussed below.

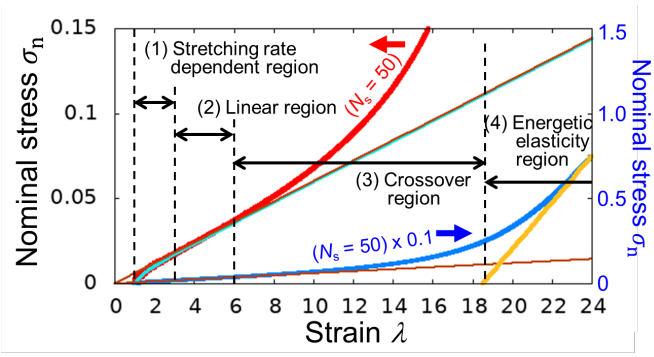

Fig. 4 Schematic of the stress-strain curve of polymer network of regular diamond lattice with N_s = 50 under $d\lambda/dt = 10^{-4}$. Two different lines (red and blue) represent the same stress-strain curve; the nominal stress σ_n of the red and blue lines is represented on the left- and right-hand-side y-axes. The four characteristic regions of the stress-strain curve are also indicated.

Confirmation of entropic and energetic elasticities

In principle, stress values in the linear entropy elastic region should be proportional to temperature (T), as well as independent of the harmonic potential's spring constant (K). Appendix E details the dependence of the stress values on T. To investigate the dependence of the stress values on K, we investigated the stress-strain curves of the regular diamond network for K = 20 under $d\lambda/dt = 10^{-4}$ and compared it with the curve for K = 40. Figure 5 shows the stress-strain curve for N_s = 100. The least squares fit provided (G, λ_u) = (0.0022847, 9.0), (0.0025461, 8.1), and (0.0025726, 8.0) for K = 20, 160 and 400, respectively. The corresponding plots for K = 160 and 400 are given in Appendix A. Thus, the values of G for K = 40, 160, and 400 were almost the same, and the ratio of the estimated G between K = 20 and 40 ($G_{K=20}/G_{K=40}$) was 1.06. This indicates that G does not depend on K and that the linear region observed here is attributable to the entropic elasticity. It is worth noting that the interaction between bonded particles in the Kremer-Grest model corresponds to a harmonic chain with K and r_0 values of 490 and 0.961, respectively, as explained in Appendix B.

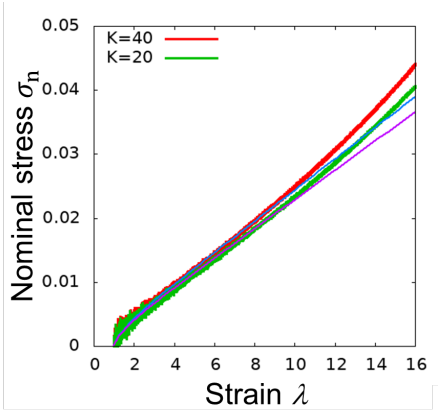

Fig. 5 Weak spring-constant dependence of stress-strain curve in the crossover region for polymer network of regular diamond lattice with K = 20 and 40 under $d\lambda/dt = 10^{-4}$, represented by green and red lines. Purple and blue lines are the fitting curves to Eq. (2) for K = 20 and 40, respectively.

A weak K-dependence was observed in the crossover regions of Figs. 5 and 10 (Appendix A). Due to the fact that this K-dependence was not proportional to K, it was ascribed to an entropic effect caused by the difference in chain stiffness rather than an energetic caused by K.

For clarifying the energetic elasticity arising from bond stretching, MD simulations with K = 20 and 40 were performed for the cases with short strands N_s = 2, 5, 10, and 25. It was expected that the deformation of the network directly affects the shorter strands. The corresponding N_t values were 20,480,

19,008, 21,000, and 26,112, respectively. Figure 6 shows the stress-strain curves for N_s = 2, 5, 10, and 25 under $d\lambda/dt = 10^{-4}$. We also performed MD simulations at T = 0.2 for N_s = 2 to clarify the temperature dependence in the high-strain region. A linear region seemingly originating from the energetic elasticity was observed in the high-strain region. Here, the energetic elastic modulus G_E was estimated from the slope of the stress-strain curve. The ratio of the energetic elastic modulus between K = 20 and 40 ($G_{E,K=20}/G_{E,K=40}$) in the high-strain region was calculated for N_s = 2 and 5; the ratios were 0.500 and 0.501, respectively. These ratios directly reflect the difference among the spring constants K = 20 and 40. Notably, as illustrated in Appendix F, the average bond length was stretched in the energetic elasticity region.

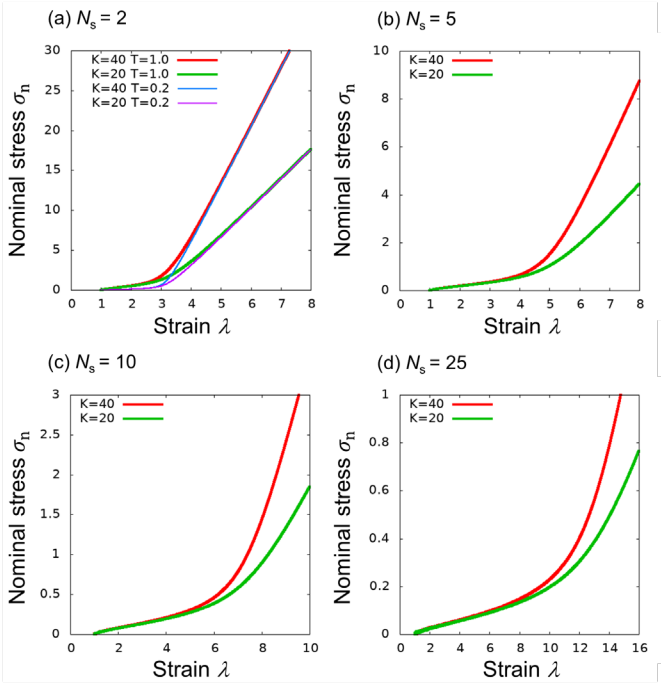

Fig. 6 Stress-strain curve of polymer network of regular diamond lattice with N_s = 2, 5, 10, and 25 under $d\lambda/dt = 10^{-4}$. Here, T = 1.0. For N_s = 2, the stress-strain curves at T = 0.2 are presented.

We try to estimate the thresholds of the linear region shown in Fig. 5 for all N_s. Table 1 shows the lower (λ_{l1} and λ_{l2}) and upper (λ_u) limit of the linear region (2) and the lower limit (λ_{E0}) of the energetic elasticity region (4) as well as the corresponding elastic moduli (G and G_E). λ_{l1} is the lower limit of the linear region (2). At the lower limit, the ratio of the stress-strain curves for stretching rates of 10^{-3} and 10^{-4} is smaller than 1.05. λ_{l2} is the lower limit of the linear region (2) as estimated for stretching rates of 10^{-4} and 10^{-5}. λ_u and G are the upper limit and shear modulus of the linear region (2), respectively. λ_{E0} is the lower limit of the energetic elasticity region (4). This value is obtained as the intersection with the x-axis. G_{E0} is the energetic elastic modulus of the energetic elasticity region (4). We confirmed that the linear region becomes wider for larger N_s, as noted by Treloar[38].

Table 1 Values of the lower (λ_{l1} and λ_{l2}) and upper (λ_u) limit of the linear region (2) and the lower limit (λ_{E0}) of the energetic elasticity region (4) as well as the corresponding elastic moduli (G and G_E).

N_s	λ_{l1}	λ_{l2}	λ_u	G	λ_{E0}	G_{E0}
2	N/A	N/A	1.30	0.27045	3.24	7.3853
5	N/A	N/A	1.69	0.10479	4.96	2.8348
10	N/A	N/A	2.30	0.046403	7.25	1.2375
25	1.74	N/A	3.97	0.014804	11.5	0.30421
50	2.70	1.65	5.1	0.0060010	18.5	0.13662
100	4.70	2.37	8.2	0.0024238	N/A	N/A
200	10.7	4.45	14.2	0.00096692	N/A	N/A

Cases with several distributions of fluctuating strand lengths

For regular diamond lattices made of linear springs, a nonlinearity appears in the entropic and energetic regions. As discussed in the previous section, the onset of this nonlinear behavior depends on N_s. When N_s fluctuates, it is expected to have a large effect on the elastic modulus and onset of nonlinearity. In this section, we evaluated the stress-strain curves of systems in which each strand length was set as a form of

$$N_s\,(\,1.0\,+\,C\,(R\,-\,0.5)\,) \qquad (5)$$

from independent uniform random numbers R between 0 and 1 with the amplitude C. This form was used simply because distributions with different characteristics are generated from one parameter, C. Moreover, this form enables us to analytically calculate the C dependence of the elastic modulus G. The behavior of G can be roughly explained by the effective spring constant k of a combination of parallel springs: $k = \sum_i k_i$, where k_i is a spring constant of the i-th spring. In the examined model, k_i is described as $k_i = a/[N_s\,(1.0 + C\,(R_i - 0.5))]$. Because R_i is a uniform random variable, the sum can be replaced by the integral of the interval [0.0, 1.0]. By using the Maclaurin series, $[\log(1 + C/2) - \log(1 - C/2)]/C$ is approximately $1 + C^2/12$ for $C \ll \sqrt{20/3}$.

To confirm the obtained theoretical prediction $(1 + C^2/12)$, we evaluated G for C = 0.5, 1.0, and 1.5. The above strand length distribution function may not directly correspond to the experimental setups of Tetra-PEG gels,[7-10,12] which use commercially available 4-arm PEGs. The commercial 4-arm PEGs (-SH / -MAL) is discrete, e.g. 2kDa, 5kDa, 10kDa, 20kDa and 40kDa. Advanced calculations for discrete 4-arm pre-polymer distributions are readily available.

Figure 7 shows the stress-strain curves for N_s = 100 and 200 with C = 0.0 (uniform N_s), 0.5, 1.0, and 1.5 under $d\lambda/dt = 10^{-4}$ and 10^{-5}. Table 2 shows (G, λ_u) obtained from the fitting to Eq. (2). The ratio of G for C = 0.5, 1.0, and 1.5 relative to that for C = 0.0 was 1.02, 1.06, and 1.14, respectively. Thus, G was approximately proportional to $1 + 0.06\,C^2$. Because C indicates the irregularity (randomness) from the regular lattice with

uniform N_s, it can be concluded that as the irregularity increases, the nonlinearity increases. Intuitively, the network with larger number of short strands exhibited stronger non-linearity. The weak discrepancy of the coefficient for C^2 is explained by rigorous theoretical calculations for a given network connection. These rigorous theoretical calculations are open problems.

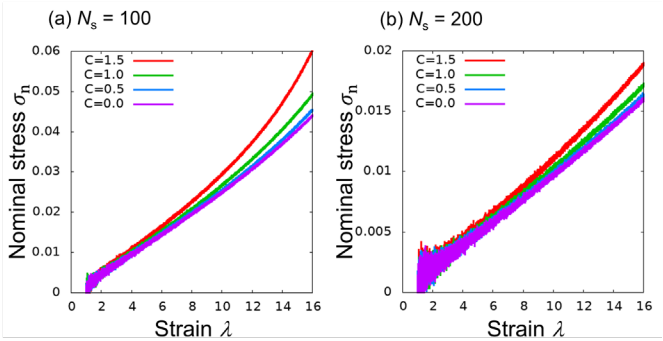

Fig. 7 Stress-strain curve of polymer network of diamond lattice with nonuniform strand length fluctuating around N_s = (a) 100 and (b) 200 under $d\lambda/dt = 10^{-4}$. Plots for $d\lambda/dt = 10^{-5}$ are shown in Appendix G.

Table 2 Fitting values of the equilibrium shear modulus G and upper limit λ_u of the linear region on the stress-strain curve.

		N_s = 100		N_s = 200	
$d\lambda/dt$	C	G	λ_u	G	λ_u
10^{-4}	0.0	0.0024238	8.2	0.00097443	14.2
	0.5	0.0024740	8.3	0.00099335	14.1
	1.0	0.0025701	8.1	0.00103301	13.3
	1.5	0.0027566	7.2	0.00110891	12.4
10^{-5}	0.0	0.0023821	8.1	0.00096692	13.3
	0.5	0.0024594	8.0	0.00098406	13.0
	1.0	0.0025478	7.4	0.00102162	12.3
	1.5	0.0027315	6.7	0.00109451	11.1

According to Sorichetti et al.,[50] the elastic modulus increased with increasing probability of shorter chains in a random network with constant functionality. As illustrated in Appendix H, the distribution of short chains increases with the increase in the value of C in the network based on Eq. (5). G's observed C-dependence could be interpreted as the result of short loops. Additionally, the details of the mechanism should be investigated further in the future.

When the molecular weight between crosslinking points is not constant but follows a widely spread distribution, the randomness increases the stress and the deviation of the upper limit strain from the linear entropic line decreases. In other words, the linear entropic region becomes small when the randomness of N_s is high.

Demonstration for different network topologies with same functionality f = 4 and uniform strand length

The previous section clarified that the distribution of strand lengths affects the stress-strain curves, that is, the elastic modulus G and onset of nonlinear behavior λ_u. This section demonstrates that the stress-strain curves can be affected by different network topologies even if the strand length is constant.

First, we investigated the BC-8 structure. The BC-8 structure for carbon has a unit cell shape for 16 carbons with a ratio of 1:1:0.977 based on the structural optimization by DFT calculations[42-45] at high pressure. In the present study, we investigated cases with both cubic and rectangular PBCs for the ratio 1:1:0.977.

For clarity, we investigate the case of a cubic PBC. Figure 8 shows the stress-strain curves of a polymer network of the BC-8 lattice elongated independently in the x-, y-, and z-directions. Here, the anisotropic direction was the z-axis, and "Top" in Fig. 1(b) corresponds to the surface perpendicular to the z-direction. In this section, the stretching rate ($d\lambda/dt$) was set to 10^{-4}. The behavior between the x- and y-directions and the z-direction was confirmed to differ owing to the anisotropy of the BC-8 structure. Further, depending on the network topology, there exist a stretching direction in which the stress increases and one in which the stress decreases. As shown in Appendix I, the results of a rectangular PBC differed slightly from those of a cubic PBC.

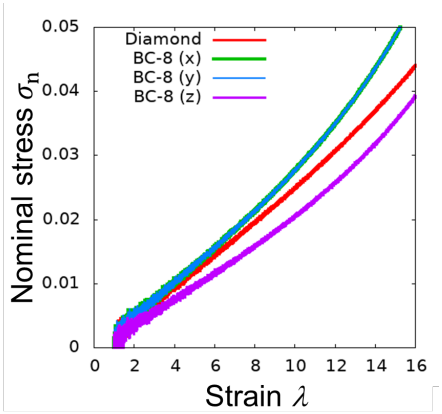

Fig. 8 Stress-strain curve of polymer network of BC-8 lattice elongated in x-, y-, and z-directions under cubic PBC with $d\lambda/dt = 10^{-4}$. Green, blue, and purple lines represent the result of BC-8 lattice stretching in x-, y-, and z-directions, respectively. For comparison, the case of diamond lattice is shown with red line.

The elastic modulus G in the x- (or y-) and z-directions were estimated from the region of linear entropic elasticity, and the ratios among the directions were calculated. Table 3 shows the fitting values of G and λ_u of the linear region on the stress-strain curve for the BC-8 network with N_s = 100. The ratios of G in the z-direction relative to that in the x- (or y-) directions were 1.34 and 1.41 times larger for cubic and rectangular PBCs, respectively. From the viewpoint of loops in the network,[13] the difference in elastic modulus between the diamond lattice and the BC-8 network was caused by the higher-order loops,

although the minimal loop of the BC-8 network was constant. The direction dependence in the BC-8 network was the same.

Table 3 Fitting values of the shear modulus G and upper limit λ_u of linear region of stress-strain curve of BC-8 network with N_s = 100, estimated under $d\lambda/dt = 10^{-4}$.

	Cubic PBC		Rectangular PBC	
	G	λ_u	G	λ_u
x-direction	0.0025928	7.3	0.0026391	7.4
y-direction	0.0025989	7.4	0.0026349	7.2
z-direction	0.0019326	7.4	0.0018753	7.5

To investigate the relationship between the elastic moduli of the entropic and energetic elasticities, the ratio of the energetic elastic modulus G_E in the x- (y-) direction relative to that in the z-direction was calculated for N_s = 2 and 5; the ratios were 1.34 and 1.32, respectively. The stress-strain curves for N_s = 2 and 5 are shown in Appendix J. The ratio for the energetic elastic modulus G_E is expected to hold even in the case with N_s = 100, because the diamond lattice case discussed above does not show the N_s dependence in the energetic elastic region. The ratios of the energetic elastic modulus G_E for N_s = 2 and 5 are very close to the ratios of the entropic elastic modulus for N_s = 100. Thus, these ratios with close values indicate that the entropic and the energetic elastic moduli G_E may be coupled through network topology. However, for the spring constant dependence of the diamond lattice shown above, the ratio ($G_{E,K=20}/G_{E,K=40}$) between K = 20 and 40 of the entropic elasticity was exceeded that of the energetic elasticity. These differences can be imagined from the comparison of the entropic and energetic elasticities between sum of two independent springs with K and a single spring with $2K$. Both represent the same force in the energetic elasticity, while the sum of two springs possesses twice the force than a single spring in the entropic elasticity. A rigorous theoretical explanation for this issue remains an open problem.

Conclusions

To investigate the linear regions of entropic elasticity as a function of the strand length N_s, we performed CGMD simulations of condensed lattice networks with harmonic bonds without the EV interactions under PBCs with a bead number density of 0.85. We observed the stress-strain curves for uniaxial stretching with stretching rates $d\lambda/dt = 10^{-3}$, 10^{-4}, and 10^{-5}. The diamond and BC-8 lattices were investigated as regular networks with functionality f = 4.

For a diamond lattice with uniform N_s = 50, 100, and 200, we found that the linear region in the stress-strain curves was wider for larger N_s. For N_s = 50, 100, and 200, the upper strain limit λ_u of the linear region was 5.1, 8.2, and 14.2, respectively. In the low-strain region, stretching rate dependence clearly existed for $d\lambda/dt = 10^{-3}$ although those for $d\lambda/dt = 10^{-4}$ and 10^{-5} were negligibly small. As a result, we found that the stress-strain curve can be divided into four regions: (1) a region depending on the stretching rate at low strain, (2) a region exhibiting linear entropic elasticity, (3) a crossover region between the entropic and the energetic regions, and (4) a region characterizing the energetic elasticity. We also confirmed the entropic elasticity of the linear region from the temperature dependence.

To investigate the effect of the network topology on the stress-strain curves, we examined the diamond lattice network with fluctuating N_s and the BC-8 lattice network with uniform N_s. Consequently, we found that the linear entropic region becomes narrower for a larger fluctuation of N_s. For the BC-8 lattice network with uniform N_s, the elastic modulus increases or decreases depending on the network connectivity (*i.e.* topology).

Conflicts of interest

There are no conflicts to declare.

Author Contributions

The manuscript was written with contributions from all the authors. Computations and analysis were mainly performed by K. H. All authors have given their approval of the final version of the manuscript.

Acknowledgements

The authors thank Prof. T. Deguchi, Dr. J. Sato, Prof. H. Jinnai, Prof. T. Kawakatsu, and Prof. T. Satoh for their useful discussions. For the computations in this work, the authors are partially supported by the Joint Usage/Research Center for Interdisciplinary Large-scale Information Infrastructures (JHPCN) and the High-Performance Computing Infrastructure (HPCI) in Japan: hp200048, hp200168, hp210132, and hp210133. This work was partially supported by JSPS KAKENHI, Japan, grant nos.: JP18H04494, JP19H00905, and JP20H04649, and JST CREST, Japan, grant nos.: JPMJCR1993 and JPMJCR19T4.

Appendix

A. Stretching rate dependence on stress-strain curves

Then, we investigated the dependence of the stress-strain curves on the stretching rate $d\lambda/dt$. Figure 9 shows the stress-strain curves under $d\lambda/dt = 10^{-4}$ and 10^{-3} (exceeding the value of 10^{-5} considered above). Here, (G, λ_u) was (0.0024238, 8.2) and (0.0025207, 11.5) for $d\lambda/dt = 10^{-4}$ and 10^{-3}, respectively. The apparent linear region seemingly widened for faster stretching. This is an artifact due to poor fitting in the low-strain region for a stretching rate of 10^{-3}. These results indicate that a sufficiently low stretching rate should be applied to evaluate the upper limit λ_u. Because the difference between ($d\lambda/dt$ =) 10^{-4} and 10^{-5} is negligible, a stretching rate of 10^{-4} is sufficient for the present study.

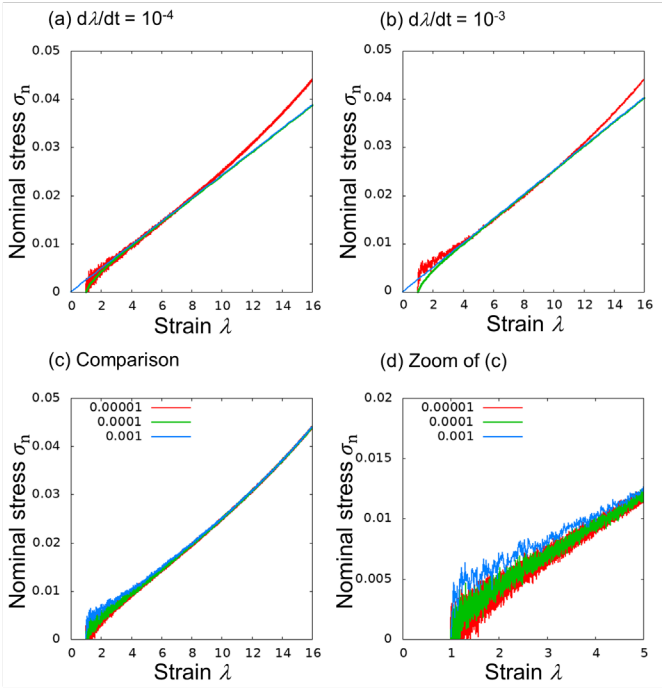

Fig. 9 Stress-strain curve of polymer network of regular diamond lattice with N_s = 100 under dλ/dt = (a) 10^{-4} and (b) 10^{-3}. Red line represents data points obtained from simulation; green line represents the fitting curve to Eq. (2); and blue line is a linear function. (c) Comparison among stretching rates (dλ/dt) of 10^{-5} (red), 10^{-4} (green), and 10^{-3} (blue). (d) Magnified view of low-strain region in (c).

Figure 9(b) with dλ/dt = 10^{-3} clearly shows the remarkable dependence of the stress-strain curves on the stretching rate (dλ/dt) in the low-strain region, although the contribution to stress was only from the bond interaction. This behavior was caused by the fast deformation compared to the relaxation time of a single strand. In uniaxial elongation with a constant engineering strain rate, the applied deformation in the higher-strain region was smaller. Thus, the stretching rate dependence in the low-strain region was more significant for larger N_s and/or faster stretching rate. It should be noted that increasing the number of ensembles to improve statistics is necessary to reduce noisy fluctuations in the region of low distortion. Because the current study is primarily concerned with the behaviors of large strain regions, only cases with dλ/dt = 10^{-4} were predominantly investigated.

Notably, these dependences differed greatly from those in the case of the Kremer-Grest model,[40] which consists of FENE bonds and LJ pairs with the EV interactions, because the EV interaction has a large effect on stress in the low-strain region. It noted that the effect of the bond potential is very weak, the difference in the function form of the bond potential has no effect, and the strength of the spring around the equilibrium has a weak effect. The dependence of the stretching rate (dλ/dt) on the stress-strain curve in the low-strain region may be negligible if only the bond contribution to stress is considered. The difference from the Kremer-Grest model is described in detail in Appendix B. The stretching rate (dλ/dt) dependence in the low-strain region was concluded to be larger for larger dλ/dt and/or larger N_s.

B. Stretching rate dependence on stress-strain curves in Kremer-Grest model

To present the strong stretching rate dependence on stress-strain curves in Kremer-Grest (KG) model[40] due to the EV interaction at the low-strain region, we performed CGMD simulations of KG model of the regular diamond lattice with the uniform arm length. Here, the initial configuration of the diamond lattice was obtained staring from expanded diamond lattice without trapped entanglements.

Before presenting the effect, we showed that the effect of bond potential is due to the spring constant around equilibrium. In addition, we clarified that the difference of function forms between the FENE and harmonic potentials has no effect. From a Taylor series expansion for a potential between bonded beads in the KG model, the coefficients (K and r_0) of the phantom chain model with harmonic bonds without the EV interactions were obtained as K = 490 and r_0 = 0.961. For comparison, we presented the distributions of the bond length as shown in Fig. 10 (a) for the cases with (K, r_0) = (40, 0.975), (160, 0.975) and (400, 0.975) in addition to that with (K, r_0) = (490, 0.961). Figure 10 (b) presents stress-strain curves with N_s =100 for (K, r_0) = (40, 0.975), (160, 0.975), (400, 0.975) and (490, 0.961). The least squares fit provided (G, λ_u) = (0.0025461, 8.1) and (0.0025726, 8.0) for K = 160 and 400, respectively.

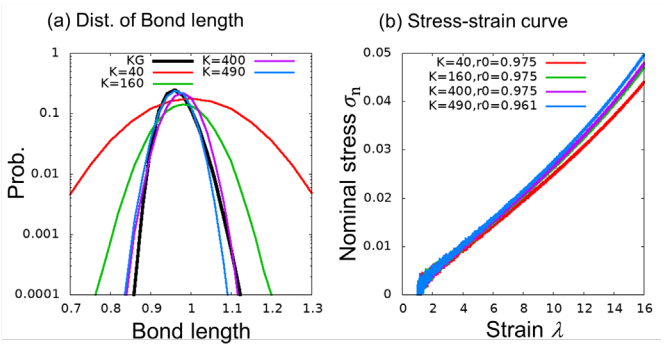

Fig. 10 Distributions of bond length and stress-strain curves for the phantom chain models with (K, r_0) = (40, 0.975), (160, 0.975), (400, 0.975) and (490, 0.961). Here, the size of each bin is 0.05. In (a), the distribution for the KG model was presented for comparison.

Figure 11 shows stress-strain curves of the KG model with N_s = 10, 25, 50, and 100 for dλ/dt = 10^{-3}, 10^{-4}, and 10^{-5}. Here, the nominal stresses of the phantom chain model were scaled with the factor of 0.6 for all N_s. This universal constant will be understood by the microscopic characteristic of the model. Research in this direction is open problem. For dλ/dt = 10^{-3} and 10^{-4}, strong dependence of stretching rate dλ/dt was observed

at the low-strain region. The overshoot observed in the stress-strain curve of the KG model was more apparent in the higher stretching rate. This artificial overshoot was originated from the collisions of the beads under rapid drawings out from a blob of strands. For the high-strain region, the stress-strain curves were in good agreement between the KG and phantom chain models. However, this high strain value exceeds the entropic linear region determined from Eq. (2). Namely, the KG model with $N_s \leq 100$ does not show the linear entropic elasticity.

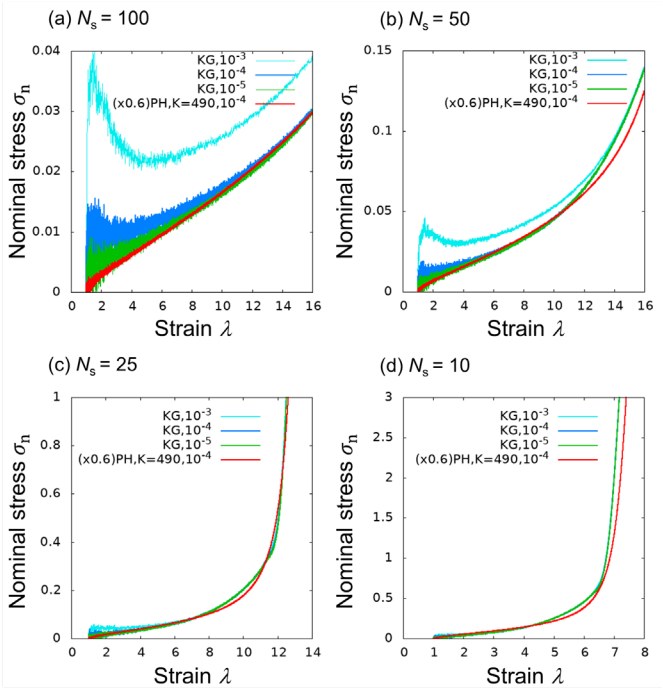

Fig. 11 Stress-strain curves of the Kremer-Grest model ($d\lambda/dt$ = 10^{-3}, 10^{-4}, and 10^{-5}) and the phantom chain model with (K, r_0) = (490, 0.961) ($d\lambda/dt$ = 10^{-4}). The nominal stress of the phantom chain model is multiplied by 0.6 for comparison.

C. Density Dependence of on stress-strain curves

The value of the number density ρ can be set arbitrarily for the network model that excludes volume interaction between non-bonding particles. Thus, a ρ value of 0.85 is commonly used as the standard value for the Kremer-Grest model, which is frequently used to describe polymer melts and cross-linked rubbers. Additionally, a decrease in the value of ρ corresponds to the expansion of the network. As a result, the strain value associated with the transition from entropy elasticity to energy elasticity is expected to be smaller for a reduced ρ value.

To further understand the ρ-dependence on the stress-strain curve, networks with a ρ value of 0.1 and 0.3 were investigated. The stress-strain curves for ρ = 0.1, 0.3, and 0.85 under stretching with $d\lambda/dt$ = 10^{-4} are shown in Figure 12. As the value of ρ decreased, the apparent linear region became narrower. This is because decreasing the density equates an expansion in the network. Thus, cases with a ρ value of 0.85 were predominantly investigated. Notably, the elastic module in the low strain region became smaller for a reduced ρ value. This was consistent with the behavior observed by Sorichetti et al.[50] in the low strain region.

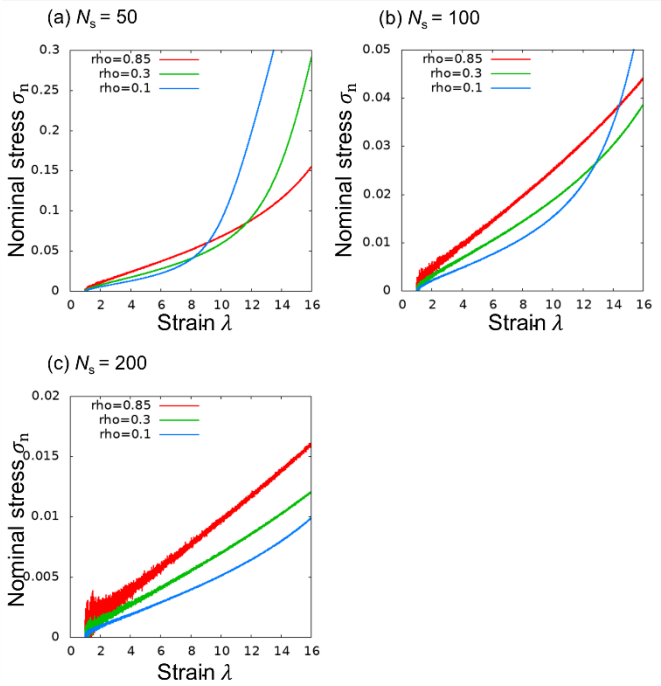

Fig. 12 Density dependence on the stress-strain curves of a regular diamond lattice polymer network under $d\lambda/dt$ = 10^{-4}, with ρ = 0.1, 0.3, and 0.85 and N_s = 50 (a), 100 (b), and 200 (c).

D. Stress-strain curves of a stretched single chain

We evaluated stress-strain curves of a stretched single chain wrapping the PBC box as shown in Fig. 13 (a). At unelongated state, size L of the PBC box is set to the average of the strand length of the regular diamond lattice with the uniform arm length. Here, L = 4.258, 5.355, and 6.742, for N = 50, 100, and 200, respectively. The PBC box was deformed with the rate of $d\lambda/dt$ = 10^{-4}. Figure 13 (b)-(d) presented the stress-strain curve for the phantom chain models with harmonic bonds and KG model. For the phantom chain model with (K, r_0) = (40, 0.975), λ_u was 5.0, 7.2, and 10.1 for N = 50, 100, and 200, respectively. Here, λ_u denotes the upper limit of the strain range to fit Eq. (2). We found that the obtained λ_u was proportional to root square of N.

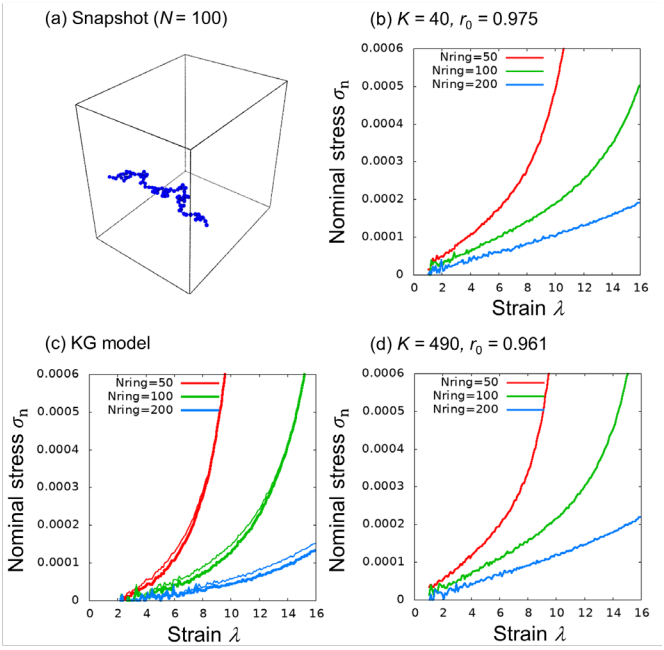

Fig. 13 Snapshot of a stretched single chain (a) and stress-strain curves with the phantom chain model (b) with (K, r_0) = (40, 0.975), the KG model (c), and the phantom chain model (d) with (K, r_0) = (490, 0.961). Here, in (c), thin lines were stress contributed only from potentials among bonded beads.

E. Stretching rate dependence on stress-strain curves

As a test for entropic elasticity, we evaluated the temperature dependence of the equilibrium shear modulus G and upper limit λ_u for T = 0.2, 0.5, and 1.0 on the regular diamond lattice. Entropic elasticity is defined here as the part of elasticity that is proportional to temperature. Figure 14 shows the stress-strain curves for T = 0.2, 0.5, and 1.0. From the fitting to Eq. (2), (G, λ_u) = (0.00052053, 9.9) and (0.0012633, 9.3) for T = 0.2 and 0.5, respectively. The values of G for T = 0.2, 0.5, and 1.0 show a linear relation described by G = 0.0024169 T with the R-squared value R^2 = 0.99926. The upper limit λ_u is almost constant. From the perfectly linear relationship of $G(T)$, the observed linear region was concluded to be holding the entropic elasticity. In addition, we also obtained a linear relation of G = 0.0060557 T and G = 0.00098442 T for N_s = 50 and 200, respectively. Here, for N_s = 50, (G, λ_u) = (0.0012846, 6.0) and (0.0031113, 5.5) for T = 0.2 and 0.5, respectively; for N_s = 200, (G, λ_u) = (0.00021056, 13.1) and (0.00050673, 5.5) for T = 0.2 and 0.5, respectively. As a result, the relation $G = AT/N_s$ with coefficient A = 0.28611 was confirmed. It is noted that N_s is proportional to the squared radius of gyration of a strand without constraints. The obtained linear relation is consistent with Hooke's law deduced from the one-dimensional model in statistical physics.

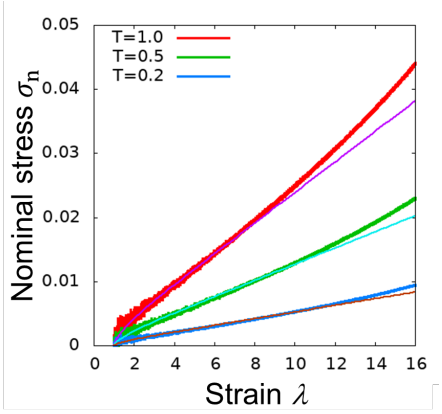

Fig. 14 Temperature dependence of stress-strain curve of polymer network of regular diamond lattice with T = 0.2, 0.5, and 1.0 under $d\lambda/dt = 10^{-4}$, represented by blue, green, and red lines. Brown, light-blue, and purple lines are the fitting curves to Eq. (2) for T = 0.2, 0.5, and 1.0, respectively.

F. Bond length distribution

To confirm that averaged bond lengths are constant in the entropic elastic region, we evaluated the distribution of bond lengths. Figure 15 presents distributions of the bond length for several strain values λ in the cases with N_s = 100 and 5. For N_s = 100, the distributions were not changed. This behavior is typical of entropic elasticity. On the other hand, for N_s = 5, remarkable shifts were observed for large strains. Averaged bond lengths b_{ave} for λ = 5.5, 6.0, 6.5, and 7.0 were 1.151, 1.226, 1.311, and 1.401, where the linear relation b_{ave} = 0.1667 λ + 0.2304 holds with R^2 = 0.9983.

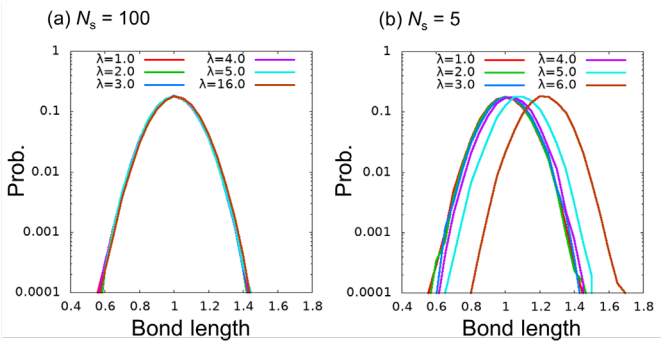

Fig. 15 Probability distribution of the bond length for the cases with (a) N_s = 100 and (b) N_s = 5. Here, the size of each bin is 0.05.

G. Stress-strain curve of polymer network of the diamond lattice with nonuniform strand length fluctuating around N_s =100 and 200 under the stretching rate of 10^{-5}

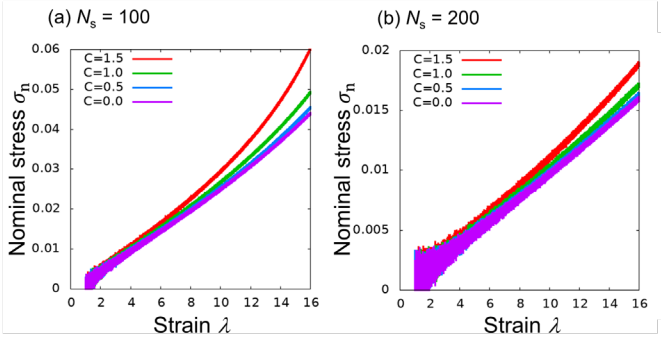

Fig. 16 Stress-strain curve of polymer network of diamond lattice with nonuniform strand length fluctuating around N_s = (a) 100 and (b) 200 under $d\lambda/dt = 10^{-5}$.

H. Distribution of the loop length for the cases with fluctuating strand length

The minimal loop in the diamond lattice network contains six bonds (constant). Thus, the loop length distribution is Gaussian in nature, as the loop length is the sum of six uniform random numbers distributed around the averaged value. Additionally, C denotes the standard deviation of this Gaussian distribution. Figure 17 illustrates the probability distribution of the loop length of the minimal loop consisting of six bonds using actual counting. The probability of the shorter chains was found to be larger for larger C.

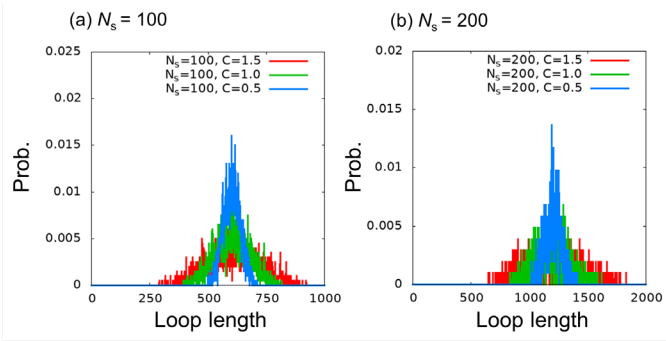

Fig. 17 Probability distribution of the loop length of the minimal loop consisting of six bonds.

I. Stress-strain relations for the BC-8 polymer network in the rectangular PBC

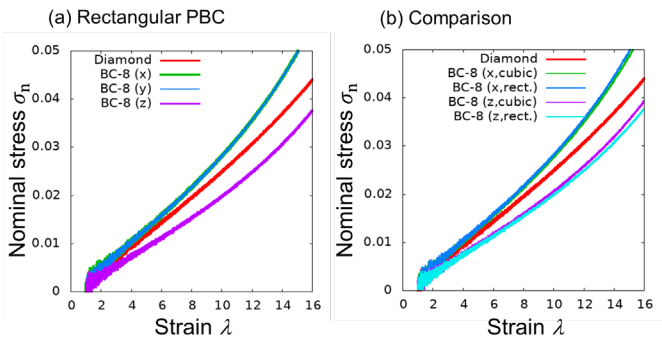

Fig. 18 Stress-strain curves of polymer network of the BC-8 lattice elongated to x-, y-, and z-direction under the rectangular PBC under $d\lambda/dt = 10^{-4}$ (a). In (b), the difference between the stress-strain curves on the rectangular and cubic lattices are focused. The stress-strain curve on the diamond lattice (under the cubic PBC) is presented in (a) and (b) for reference.

J. Energetic elasticity of the BC-8 polymer network with N_s = 2 and 5

From a linear fitting for high strain region, we obtained $\sigma_n = 7.59\ \lambda - 19.72$, $\sigma_n = 5.66\ \lambda - 14.71$ for $N_s = 2$, and $\sigma_n = 2.84\ \lambda - 10.95$, $\sigma_n = 2.15\ \lambda - 8.47$ for $N_s = 5$. The ratio of G in the z-direction relative to that in the x- (or y-) directions was 1.34 and 1.32 for N_s = 2 and 5, respectively.

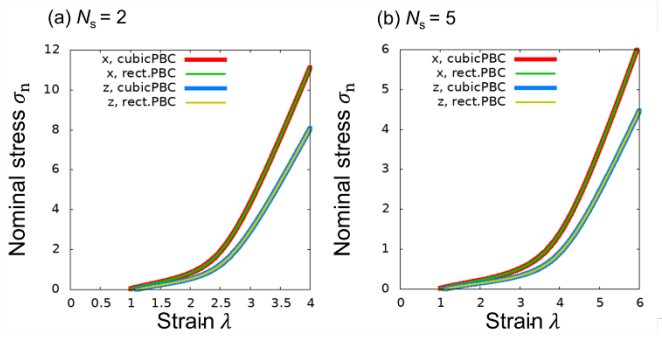

Fig. 19 Stress-strain curve of polymer network of the regular diamond lattice with N_s = 2 and 5 under the cubic and rectangular PBC. Here, the stretching rate ($d\lambda/dt$) was 10^{-4}.

Notes and references

1 M. Doi, S. F. Edwards, The theory of polymer dynamics, Clarendon Press, Oxford, 1986.
2 P. G. De Gennes, Introduction to polymer dynamics, Cambridge University Press, New York, 1990,
3 G. R. Strobl, The physics of polymers: Concepts for understanding their structures and behavior, Springer-Verlag, New York, 1996.
4 B. Erman, J. E. Mark, Structures and Properties of Rubberlike Networks, Oxford University Press, Oxford, 1997.
5 M. Rubinstein, R. H. Colby, Polymer Physics, Oxford University Press, Oxford, 2003.
6 T, Isono, T. Satoh, private communication.

7 T. Sakai, T. Matsunaga, Y. Yamamoto, C. Ito, R. Yoshida, S. Suzuki, N. Sasaki, M. Shibayama, U.-i. Chung, *Macromolecules* 2008, **41**, 5379.
8 T. Sakai, Y. Akagi, T. Matsunaga, M. Kurakazu, U.-i. Chung, M. Shibayama, *Macromol. Rapid Commun.* 2010, **31**, 1954.
9 M. Shibayama, *J. Phys. Soc. Jpn.* 2009, **78**, 041008.
10 M. Shibayama, *Soft Matter* 2012, **8**, 8030.
11 P. Pincus, *Macromolecules*, 1976, **9**, 386.
12 T. Katashima, K. Urayama, U.-i. Chung, T. Sakai, *J. Chem. Phys* 2015, **142**, 174908.
13 M. Zhong, R. Wang, K. Kawamoto, B. D. Olsen, J. A. Johnson *Science* 2016, **353**, 1264.
14 T.-S. Lin, R. Wang, J. A. Johnson, B. D. Olsen, *Macromolecules* 2018, **51**, 1224.
15 T.-S. Lin, R. Wang, J. A. Johnson, B. D. Olsen, *Macromolecules* 2019, **52**, 1685.
16 M. Lang, *ACS Macro Lett.* 2018, **7**, 536.
17 M. Lang, *Macromolecules*, 2013, **46**, 1158.
18 M. Lang, *Macromolecules*, 2017, **50**, 2547.
19 M. Lang, *Macromolecules*, 2019, **52**, 6266.
20 M. Lang, T. Müller, *Macromolecules* 2020, **53**, 498.
21 S. Panyukov, *Polymers*, 2020, **12**, 767.
22 S. Panyukov, *Macromolecules*, 2019, **52**, 4145.
23 W. Kuhn, *Angew. Chem.* 1936, **49**, 858.
24 W. Kuhn, *J. Poly. Sci.* 1946, **1**, 380.
25 P. J. Flory, *J. Chem. Phys.* 1943, **11**, 512.
26 H. M. James, E. Guth, *J. Chem. Phys.* 1943, **11**, 455.
27 H. M. James, E. Guth, *J. Chem. Phys.* 1947, **15**, 669.
28 P. J. Flory, *Proc. R. Soc. London, Ser. A* 1976, **351**, 351.
29 R. Everaers, *New J. Phys.* 1999, **1**, 12.
30 R. Everaers, K. Kremer, *Macromolecules* 1995, **28**, 7291.
31 R. Everaers, K. Kremer, *Phys. Rev. E* 1996, **53**, R37.
32 G. S. Grest, M. Pütz, R. Everaers, K. Kremer, *J. Non-Cryst. Sol.* 2000, **274**, 139.
33 E. R. Duering, K. Kremer, G. S. Grest, *J. Chem. Phys.* 1994, **101**, 8169.
34 A. A. Gusev, *Macromolecules* 2019, **52**, 3244.
35 A. A. Gusev, F. Schwarz, *Macromolecules* 2019, **52**, 9445.
36 I. C. Tsimouri, F. Schwarz, W. Caseri, P. J. Hine, A. A. Gusev, *Macromolecules* 2020, **53**, 5371.
37 M. Toda, H. Morita, *AIP Advances* 2018, **8**, 125005.
38 L. Treloar, *Trans. Faraday Soc.* 1945, 42, 83-94.
39 S. Plimpton, *J. Comp. Phys*. 1995, **117**, 1-19.
40 K. Kremer, G. S. Grest, *J. Chem. Phys.* 1990, **92**, 5057-5086.
41 P. Giannozzi, et. al. *J. Phys.: Condens. Matter* 2009, **21**, 395502.
42 M. Yin, *Phys. Rev. B* 1984, **30**, 1773.
43 A. A. Correa, S. A. Bonev, G. Galli, *Proc. Natl. Acad. Sci.* 2006, **103**, 1204.
44 K. Hagita, R. Sahara, Y. Kawazoe, *J. Chin. Chem. Soc.* 2016, **63**, 526.
45 L. Rapp, B. Haberl, C. J. Pickard, J. E. Bradby, E. G. Gamaly, J. S. Williams, A. V. Rode, *Nat. Comm.* 2015, **6**, 1.
46 T. Sunada, *Not. Am. Math. Soc.* 2008, **55**, 208. Correction, *Not. Am. Math. Soc.* 2008, **55**, 343.
47 M. W. Matsen, F. S. Bates, *Macromolecules* 1996, **29**, 7641.
48 D. A. Hajduk, R. E. Harper, S. M. Gruner, C. C. Honeker, E. L. Thomas, L. J. A. Fetters, *Macromolecules*, 1995, **28**, 2570.
49 M. O'Keeffe, M. A. Peskov, S. J. Ramsden, O. M. Yaghi, *Acc. Chem. Res.* 2008, **41**, 1782.
50 V. Sorichetti, A. Ninarello, J. M. Ruiz-Franco, V. Hugouvieux, W. Kob, E. Zaccarelli, and L. Rovigatti, *Macromolecules* **2021**, 54, 3769.

